SLAC-PUB-6324
SLAC/SSRL-0045
August 1993
(SSRL-M)

TESTS OF VARIABLE-BAND MULTILAYERS DESIGNED FOR INVESTIGATING OPTIMAL SIGNAL-TO-NOISE VS. ARTIFACT SIGNAL RATIOS IN DUAL-ENERGY DIGITAL SUBTRACTION ANGIOGRAPHY (DDSA) IMAGING SYSTEMS*

D. Boyers, A. Ho, Q. Li, M. Piestrup, M. Rice†, R. Tatchyn†

Adelphi Technology Inc, 2181 Park Blvd, Palo Alto, CA 94306

Stanford Linear Accelerator Center, Stanford Synchrotron Radiation Laboratory,
Stanford University, Stanford, California, 94309†

Abstract

In recent work, various design techniques were applied to investigate the feasibility of controlling the bandwidth and bandshape profiles of tungsten/boron-carbon (W/B_4C) and tungsten/silicon (W/Si) multilayers for optimizing their performance in synchrotron radiation based angiographical imaging systems at 33 keV. Varied parameters included alternative spacing geometries, material thickness ratios, and numbers of layer pairs. Planar optics with nominal design reflectivities of 30 % - 94 % and bandwidths ranging from 0.6 % - 10 % were designed at the Stanford Synchrotron Radiation Laboratory, fabricated by the Ovonic Synthetic Materials Company, and characterized on Beam Line 4-3 at the Stanford Synchrotron Radiation Laboratory. In this paper we report selected results of these tests and review the possible use of the multilayers for determining optimal signal to noise vs. artifact signal ratios in practical Dual-Energy Digital Subtraction Angiography systems.

Presented at the 8th National Conference on Synchrotron Radiation Instrumentation,
Gaithersburg, Md, August 23-26,1993

*Supported by DOE Offices of Basic Energy Sciences and High Energy and Nuclear Physics and Department of Energy Contract DE-AC03-76SF0015.

1. Introduction

The clinical quality of angiograms generated at the iodine K edge (33 keV) with conventional Dual Energy Digital Subtraction Angiography (DDSA) systems using synchrotron radiation (SR) has been limited from the outset in a number of respects [1,2]. Contributing factors include: 1) a low-to-moderate signal to noise (S/N) ratio stemming from the finite number of photons per pixel; 2) resolution limitations stemming from low pixel density; 3) loss of resolution due to heart motion; and 4) loss of resolution from transmitted harmonics. Since each of these limitations can be overcome to a greater or lesser extent by increasing the fundamental in-band (33 keV) photon flux, various schemes for accomplishing this have been considered or attempted. These have included: 1) increasing the efficiency (i.e., response) of the detector system to 33 keV photons while increasing harmonic rejection [3,4,5]; 2) increasing the total flux from wiggler sources while operating at critical energies significantly below 33 keV to decrease the harmonic flux relative to 33 keV [6]; 3) substituting short-period undulators for wigglers [7]; 4) improving the duty cycle of the optical system [8]; and 5) increasing the bandwidth of the monochromatized above- and below-edge spectral lines [9,10,11].

In implementing the "increased bandwidth" approach, the gain in the S/N ratio (nominally proportional to the square root of the relative increase in bandwidth) becomes limited by the appearance of images of non-iodinated body parts (bone, cartilage, etc.), whose contrast increases in some proportion to both the bandwidths of the near-edge lines, as well as to their increasing separation. A still-undetermined experimental question is the signal levels at which these undesired "artifact" images can begin to annul the increased clinical information content of the angiogram stemming from the overall increase in flux.

In the research reported in this paper, we have systematically considered and tested the use of multilayer optics as a means of increasing the bandwidths and modulating the bandshapes of the near-edge DDSA lines in the vicinity of 33 keV. A primary motivation has been the development of reliable techniques for manufacturing high-quality optics that could be used to experimentally investigate the clinical tradeoffs between, e.g., increased S/N and enhanced artifact images. Another motivation is the eventual utilization of these optics as monochromator elements. With these purposes in mind, we have developed multilayer reflectors ranging in bandwidth from approximately 0.5 % to 10 % and have conducted computer simulations of iodinated phantom models to obtain insight into real DDSA imaging systems. In the following sections we will briefly summarize selected results of our research and discuss possible applications to systematic imaging studies and practical DDSA monochromator systems.

2. Variable-band multilayers: design

The multilayer structure (hereinafter "default structure") on which our work is based consists of N repeating layer-pairs of thickness d, each composed of one high-Z and one low-to-moderate-Z material.

3

The differential scattering power of the two materials introduces a phase shift per layer-pair which, when repeated N times, can cause constructive interference and enhanced scattering in a direction approximately equal to the angle of radiation incidence. Real-time control of the fabrication process parameters and materials in multilayer construction allows for the consideration of structures whose periodicity, regularity, local composition, and local/global physical and optical properties can be adjusted in a number of ways. This richness of adjustable parameter space leads naturally to the notion of tailoring the structure of a default multilayer for a specific optical (or other physical) application. In prior work, for example, a number of structural modifications of a conventional, uniform-period configuration have been proposed both for optimizing reflectivity in the x-ray range (where absorption effects can be significant) and for increasing the bandwidth of the reflectivity peak [12,13,14]. For the present research, in which control of both of these characteristics was sought, we have investigated the following design stratagems [11,15]: 1) gradual monotonic increase or decrease of the d-spacing of a default structure (see Fig. 1), hereinafter referred to as "continuous" or "quasi-continuous" grading; 2) "cluster" grading, viz., a succession of default multilayers, each deposited successively, with an incremental increase (or decrease) of the d-spacing of each default structure (see Fig. 2); 3) "cluster/etalon" grading, viz., cluster grading with etalon spacers deposited between successive default structures; 4) "variable ratio" structures, in which the thicknesses of the high-Z vs. low-Z multilayer materials in each period d of a default (or continuously graded or cluster graded) structure is incrementally increased or decreased ; 5) default structures with differing high-Z vs low-Z thickness ratios; 6) arbitrary structures with varying numbers of layer-pairs; and 7) arbitrary structures with different high-Z vs low-Z materials.

The design options were investigated with analytical simulation programs developed by one of us (R. T.) at SSRL. These are based on a self-consistent dynamical scattering formalism related to the matrix method of Florin Abeles [16]. With negligible interfacial roughness between the multilayer materials the programs yield results approximately valid for periodic arrays of homogeneous planar slabs, each characterized by the averaged complex index of refraction of the slab material. For sufficiently small-scale and normally distributed interfacial roughness, the ideal (homogeneous slab) reflectivity is conventionally corrected by the geometrically derived scalar multiplier

$$\eta \cong \exp\left\{-\left(\frac{4\pi\sigma\sin\theta}{\lambda}\right)^2\right\}, \qquad (1)$$

where θ is the angle of incidence on the multilayer, σ is the standard deviation of the interfacial roughness distribution, and λ is the wavelength of the Bragg-diffracted light [17]. The programs utilized in the present work also utilize the same σ parameter, but employ a more detailed representation of the scattering process that is not in general representable by a simple scalar multiplier. Calculated reflectivity curves for a 10 % bandwidth (BW) W/B_4C multilayer with, respectively, σ = 0 Å and σ = 3.5 Å are

shown in Fig. 3. A more detailed discussion of the modeling and parameter studies on which the present work is based can be found in prior references [11,15].

In may be useful to note that, although a large number of variations of a default multilayer structure have been theoretically investigated by us, many other potentially interesting modifications remain to be studied. As an example, optimization of the higher reflectivity orders by utilizing periodic or quasi-periodic structures with three or more repeating materials could be explored, or the use of electrically or magnetically polarizable materials for controlling the reflectivity or transmissivity response to polarized light could prove to be important. Lateral (as opposed to depth-dependent) variation of all the parameters considered here could also lead to optimal structures for specific applications. As may be easily inferred, a basic direction in multilayer design suggested by the present work is the detailed control of the band-shape, viz., the local amplitude *and* slope of the reflectivity profile (as opposed to the simple maximization of the reflectivity peak or its full-width half-maximum (FWHM) BW).

3. Variable-band multilayers: fabrication and testing

Effects of substrate flatness and roughness on the local interfacial and overall global quality of multilayers have been studied for many substrate and multilayer materials [18,19,20,21]. Studies of the effect of the absolute thicknesses of the high-Z or low-Z multilayer materials on these parameters have been carried out for selected elements as well [22]. For the materials utilized in our experiment (tungsten (W), silicon(Si), and boron-carbon (B_4C)), previously reported behavior indicated that minimizing substrate roughness would in general tend to minimize or improve the interfacial roughness. Considerations related to the reduced effect of interfacial roughness on the peak reflectivity vs the reduction of incidence angle (and increased multilayer length) with increased d spacing led us to select d values in the 18 Å - 23 Å range. In a first fabrication run carried out in part to explore the effects of substrate quality on the multilayer performance, W/B_4C samples of various bandwidths and bandshape profiles were designed and fabricated on two types of substrate: 1) 3 inch diameter, 25 mil thick polished Si wafers (measured local rms roughnesses ranging from 2 Å - 9 Å); and 2) 1 inch diameter, 3 mm thick Zerodur (< 1.2 Å rms roughness). The bandwidths of the samples were designed assuming a 3.5 Å interfacial roughness in the: 1) default, 2) continuously-graded, and 3) cluster-graded structures. This parameter was drawn from results reported from prior sputter-deposition efforts by the Ovonic Synthetic Materials Company (Ovonics) and other workers [23,24] investigating tungsten/lower-Z material systems.

Following fabrication, Ovonics characterized the structures' reflectivities with a conventional 8 keV (copper (Cu) K_α) tube source . At SSRL, the samples' absolute reflectivities as a function of incidence angle were characterized on Beam Line 4-3 in the geometry shown in Fig. 4. Most of the samples deposited on the Si wafers exhibited substantially poorer performance than predicted from the assumed

design parameters, with the discrepancies accountable by either the large or irregular interfacial roughnesses, poor and non-repeatable local flatness effects, or both. In contrast, the Zerodur samples exhibited substantially improved agreement with the theoretical designs. An overlay of the designed and measured reflectivity profiles of a 10% BW continuously-graded multilayer on Zerodur is shown in Fig. 5. The centroid and reflectivity profile of the calculated curve have been shifted and scaled by, respectively, 3 % and 7 % (increase) to agree with the centroid and peak reflectivity of the measured profile.

Following the analysis of our first run results, a second ("Phase II") batch of samples was designed and prepared. Since satisfactory results in adjusting the bandwidth by grading the periodicity were obtained in the first run, the emphasis in the design of the second set was placed primarily on modulating the reflectivity's BW by adding Si to our materials roster and varying [15]: 1) the thickness ratio of the high-Z vs low-Z materials; 2) the number of layer-pairs N; and 3) the size of the period (d) of a default multilayer configuration. For the production run thicker and larger Si substrates, with dimensions and specified surface roughnesses listed in Table 1, were prepared by General Optics. Following characterization of the completed multilayers at Cu K_α by Ovonics, they were comprehensively tested at 33 keV on beam line 4-3 at SSRL. $\theta - 2\theta$ (absolute reflectivity), x-direction (at fixed θ and 2θ), energy (at fixed θ and 2θ), and θ (at fixed 2θ) scans were performed on selected samples, with the θ - 2θ scans taken for all the samples. A list of selected samples, together with their measured reflectivities and bandwidths, is given in Table 2.

4. Applications of variable-band multilayers to DDSA imaging tests and instrumentation

Using software developed in part at Adelphi Technology, we have simulated the detection of images of iodinated arteries imbedded in material matrices with the absorptivity properties of the human body. In Figure 6 a set of representative curves reflecting the different parameters of a typical simulation are shown. In the top graph, the effect on S/N of separating the above- and below-edge DDSA lines for four line bandwidths is shown. The signal for each line is defined independently as stemming from the net absorbtance of the body with iodination minus its absorptance without iodination. For each curve the same total number of integrated photons has been assumed, making it evident that increasing line bandwidth and separation while maintaining a net constant flux would be deleterious to S/N. In actuality, of course, for a conventional DDSA photon source the integrated flux for each curve will increase proportionately to its bandwidth, yielding a potentially significant net increase in S/N (e.g., the peak of the 10% curve in the top graph would be approximately 12 times that of the 0.5% peak). This trend alone, however, is ultimately limited by the increased manifestation of specific artifacts, e.g., bone, as the line separation is increased. In the middle graph, the simulated ratio of the signal from the iodinated arteries to the body's in-line bone content is plotted for the same four lines as in the top graph. It is now evident

that the intrusion of bone artifacts is a strong function of increasing energy separation: for the particular case shown, for example, a line energy separation of > 2 % for line BWs of > 2 % would always yield an artery/bone signal ratio of < 1. In the bottom graph a (solid) contour indicating the required number of photons/pixel to maintain a S/N ratio of at least 4 and an artery/bone signal ratio of at least 1 is plotted as a function of line BW. For the reason just cited, this contour does not extend beyond the rightmost limit of the abscissa. The dotted line, representing the photon flux from a typical source (passed by a multilayer and the patient's body) vs the multilayer's bandwidth, locates an optimal operating BW of about 1.2 %.

Although studies such as these may account for many of the essential features of DDSA systems and generally corroborate the theoretical assessments of other workers [9,25,26], it should be evident that our model assumptions and the values we assigned to our simple signal-to-noise and artery-to-bone imaging criteria are as yet insufficiently substantiated to rigorously define the optimal operating point of a real DDSA system. To date, unfortunately, high quality diffractive optics in the $\approx$0.5% - 10 % BW range have been unavailable to perform this type of investigation. In view of this, it is our belief that a valid way to assess the clinically relevant tradeoffs associated with increasing the bandwidth and separation of the DDSA lines would be to employ the multilayers developed by us in actual imaging studies.

An additional direction made possible by our work is the development of monochromator configurations employing variable-band optics both for angiography applications and other purposes [27]. At the time of this writing, the alternative methods of using bent or mosaic crystals [9,10,28] to enhance bandwidth are evidently superseded in certain respects by our approach. The first method, for example, is presently limited to a BW of about 0.5 %, while mosaic-crystal structures reportedly exhibit inferior focusing/imaging properties. A singular characteristic of a multilayer monochromator in this range (in contrast to ones based on natural crystals) is, of course, the much smaller angle of incidence and scattering. Despite this constraint, we have developed in-principle designs suitable for operation on SR beam lines. In future work we plan to: 1) systematically extend our theoretical and experimental studies of variable-band multilayers; and 2) explore further DDSA applications (e.g., harmonic rejection, signal discrimination, etc.) and other uses of multilayers with controllable bandshapes.

5. Acknowledgments

Assistance from SSRL staff, in particular John Arthur and Hal Tompkins, in the execution of the experimental runs on Beam Line 4-3, is acknowledged. Discussions with James Wood and Paul Pflag of Ovonics regarding the selection of sputtering parameters for the sample fabrication are acknowledged. Portions of this research were performed at Adelphi Technology under NSF Grant ISI-9023317. Other portions were performed at SSRL and SLAC, which are operated by the Department of Energy, Offices of Basic Energy Sciences and High Energy and Nuclear Physics.

7

Table 1

Substrate specifications for Phase II samples.

Material	Quantity	Dimensions (W x L x H)	Polished Surface rms Roughness	Polished Surface Flatness
silicon	8	1"x 2"x 0.4"	1 Å	0.1 λ_{HeNe}
silicon	8	1"x 4"x 0.4"	1 Å	0.1 λ_{HeNe}
quartz*	8	1"(D) x 0.118"	2 Å	0.1 λ_{HeNe}

* the quartz substrates are round.

Table 2

Reflectivity and bandwidth (BW) of Phase II samples measured at 33 keV.

Sample Number	t_W	t_{Si}	Substrate (W x L)	# of Layer Pairs	Absolute Reflectivity	BW
1-2	6 Å	17 Å	1" x 2"	200	84 %	2.20 %
2-2	6 Å	12 Å	1" x 2"	200	59 %	0.60 %
3-2	9 Å	14 Å	1" x 2"	200	92 %	1.50 %
4-2	9 Å	9 Å	1" x 2"	200	65 %	0.90 %
	t_W	t_{Si}				
1-4	6 Å	17 Å	1" x 4"	200	41 %	3.20 %
2-4	6 Å	12 Å	1" x 4"	200	51 %	1.70 %
3-4	9 Å	14 Å	1" x 4"	200	94 %	1.30 %
4-4	9 Å	9 Å	1" x 4"	200	62 %	0.88 %
	t_W	t_{B_4C}				
5-2	6 Å	12 Å	1" x 2"	250	79 %	0.90 %
6-2	6 Å	12 Å	1" x 2"	150	72 %	0.87 %
7-2	9 Å	9 Å	1" x 2"	250	32 %	0.67 %
8-2	9 Å	14 Å	1" x 2"	200	75 %	1.80 %
	t_W	t_{B_4C}				
5-4	6 Å	12 Å	1" x 4"	250	85 %	0.90 %
6-4	6 Å	12 Å	1" x 4"	150	61 %	0.87 %
7-4	9 Å	9 Å	1" x 4"	250	54 %	0.66 %

6. References

[1] E. Burattini and A. Rindi, eds., Synchrotron Radiation Applications to Digital Subtraction Angiography (SYRDA), Italian Physical Society Conference Proceedings No. 10, Editrice Compositori, Bologna, 1988.

[2] L. Wexler, "Clinical Aspects of Intravenous DSA: Challenges for SYRDA to Overcome," ibid., p. 53.

[3] E. N. Dementyev, E. Ya. Dovga, G. N. Kulipanov, A. S. Medvedko, N. A. Mezentsev, V. F. Pindyurin, M. A. Sheremov, A. N. Skrinsky, A. S. Sokolov, V. A. Ushakov, E. I. Zagorodnikov, A. G. Kaidorin, and Yu. V. Neugodov, "First results of experiments with a medical one-coordinate x-ray detector on synchrotron radiation of VEPP-4," Nucl. Instrum. Meth. A246, 726(1986).

[4] E. Rubenstein, J. C. Giacomini, H. Gordon, A. C. Thompson, G. Brown, R. Hofstadter, W. Thomlinson, and H. D. Zeman, "Synchrotron radiation coronary angiography with a dual-beam, dual-detector imaging system," Nucl. Instrum. Meth. A291, 80(1990).

[5] H. J. Besch, E. J. Bode, R. H. Menk, H. W. Schenk, U. Tafelmeier, A. H. Walenta, and H. Z. Xu, "A high precision, high speed X-ray detector for the noninvasive coronary angiography with synchrotron radiation," Nucl. Instrum. Meth. A310, 446(1991).

[6] H. D. Zeman and H. R. Moulin, "Removal of Harmonic Artifacts from Synchrotron Radiation Coronary Angiograms," IEEE Trans. Nucl. Sci. 39(5), 1431(1992).

[7] P. L. Csonka and R. Tatchyn, "Short Period Undulators for Human Angiography," Proceedings of the Workshop on Fourth Generation Light Sources, M. Cornacchia and H. Winick, eds., SSRL Report No. 92/02, p. 555.

[8] W.-R. Dix, K. Engelke, C.-C. Glüer, W. Graeff, C. P. Höppner, K.-H. Stellmaschek, T. Wrobleweski, W. Bleifeld, K. H. Höhne, and W. Kupper, "NIKOS - a system for non-invasive examination of coronary arteries by means of digital subtraction angiography with synchrotron radiation," Nucl. Instrum. Meth. A246, 702(1986).

[9] H. D. Zeman and D. P. Siddons, "Contrast agent choice for intravenous coronary angiography," Nucl. Instrum. Meth. A291, 67(1990).

[10] P. Suortti, W. Thomlinson, D. Chapman, N. Gmür, R. Greene, and N. Lazarz, "Performance evaluation of a bent Laue monochromator," Nucl. Instrum. Meth. A297, 268(1990).

[11] R. Tatchyn, "Preliminary Design Study for a Scanning Multilayer Mirror/Monochromator System for Diagnostic Angiography at the Iodine Kα Edge," SLAC-PUB-6412.

[12] E. Spiller, "Low-Loss Reflection Coatings Using Absorbing Materials," Appl. Phys. Lett. 20(9), 365(1972).

[13] D. J. Nagel, J. V. Gilfrich, and T. W. Barbee, Jr., "Bragg diffractors with graded-thickness multilayers," Nucl. Instrum. Meth. 195, 63(1982).

[14] D. H. Bilderback, B. M. Lairson, T. W. Barbee, Jr., G. E. Ice, and C. J. Sparks, Jr., "Design of doubly

focusing, tunable (5-30 keV), wide bandpass optics made from layered synthetic microstructures," Nucl. Instrum. Meth. 208, 251(1983).

[15] R. Tatchyn, "Numerical Studies of the Peak Reflectivity and FWHM Angular Width of Uniformly Spaced Multilayers vs. d Spacing, Thickness of the High Z Element, and Number of Layer Pairs," SLAC-PUB-6413.

[16] F. Abeles, "Recherches sur la propagation des ondes electromagnetiques sinusoidales dans les milieux stratifies. Application aux couches minces," Annales de Physique, Tome 5, 1950, pp. 596-640 (Part I), pp. 707-782 (Part 2).

[17] E. Spiller, "Evaporated Multilayer Dispersion Elements for Soft X-Rays," American Institute of Physics Proceedings No. 75, 1982, p. 124.

[18] W. K. Warburton and T. W. Barbee, Jr., "Substrate surface quality effects on multilayer performance in synchrotron radiation premonochromator systems," Nucl. Instrum. Meth. A291, 237(1990).

[19] Z. Milanovic, M. A. Voelker, M. F. Kelley, K. D. Powers, and C. M. Falco, "Surface roughness healing for XUV multilayer coatings," SPIE Proceedings No. 948, 194(1988).

[20] J. M. Slaughter, P. A. Kearney, D. W. Schulze, and C. M. Falco, "Interfaces in Mo/Si Multilayers," SPIE Proceedings No. 1343, 73(1991).

[21] C. M. Falco and J. M. Slaughter, "Characterization of metallic multilayers for x-ray optics," Journal of Magnetics and Magnetic Materials 126, 3(1993).

[22] A. Fuller, R. Tatchyn, P. Csonka, and I. Lindau, "Studies of intefacial structure in WC multilayers," SPIE Proceedings No. 733, 286(1987).

[23] T. W. Barbee, Jr., "Sputtered Layered Synthetic Microstructure (LSM) Dispersion Elements," American Institute of Physics Proceedings No. 75, 1982, p. 131.

[24] James Wood, Ovonic Synthetic Materials Company, Troy, Michigan, private communication.

[25] G. N. Kulipanov, N. A. Mezentsev, V. F. Pindurin, A. N. Skrinsky, M. A. Sheromov, A. P. Ogirenko, and V. M. Omigov, "Application of synchrotron radiation to the study of man's circulatory system," Nucl. Instrum. Meth. 208, 677(1983).

[26] A. Q. R. Baron, T. W. Barbee, Jr., G. S. Brown, "A Multilayer Monochromator for Synchrotron Radiation Angiography," SPIE Proceedings No. 1343, 230(1991).

[27] R. Tatchyn, "Variable-band multilayers as optimized reflectors for x-ray flourescence based trace impurity analysis," SLAC-PUB-6413.

[28] W. Thomlinson, N. Gmür, D. Chapman, R. Garrett, N. Lazarz, H. Moulin, A. C. Thompson, H. D. Zeman, G. S. Brown, J. Morrison, P. Reiser, V. Padmanabahn, L. Ong, S. Green, J. Giacomini, H. Gordon, E. Rubenstein, "First operation of the medical research facility at the NSLS for coronary angiography," Rev. Sci. Instrum. 63(1), 625(1992).

8. Figure captions

Figure 1. "Continuously" graded multilayer geometry with period $d_n (= t_A + t_B + n\varepsilon_A + n\varepsilon_B)$ increasing toward substrate. The subscripted symbol $\tilde{n}_i$ represents the complex index of refraction of material i.

Figure 2. "Cluster" graded multilayer geometry with a total of N/M uniform-period multilayers deposited successively on top of one another.

Figure 3. Calculated reflectivity vs angle of incidence for a W/B_4C continuously graded multilayer designed for a 10 % BW at 33 keV. Curve A: reflectivity with 0 Å interfacial rms roughness. Curve B: reflectivity with 3.5 Å interfacial rms roughness.

Figure 4. Experimental θ - 2θ scanning configuration on Beam Line 4-3 on SPEAR for measuring the absolute reflectivity of multilayers deposited on silicon (and Zerodur) substrates. For the normalizing measurement, the multilayer is lowered to allow the detector to read the monochromatized probe radiation at $2\theta=0$.

Figure 5. Measured 33 keV reflectivity curve of a W/B_4C 10 % BW multilayer overlaid on an earlier calculated curve of a similar structure with an assumed 3.5 Å interfacial rms roughness (Curve B, slightly scaled and shifted, of Fig. 4).

Figure 6. DDSA studies of the effects of increased bandwidth and separation of the above- and below-edge spectral lines. Graph (a) shows the effects of increased line separation on the S/N ratio for lines with four different bandwidths (BW), each transmitting the same total number of photons. Graph (b) shows the ratio of the signal from the iodinated artery to the bone artifact signal for the same four lines. Graph (c) shows a contour (solid line) representing the number of photons/pixel required for operation at a S/N ratio of 4 and an artery/bone signal ratio of 1. The dotted line, representing the flux vs bandwidth transmitted by a multilayer, identifies the optimal operating bandwidth of the system.

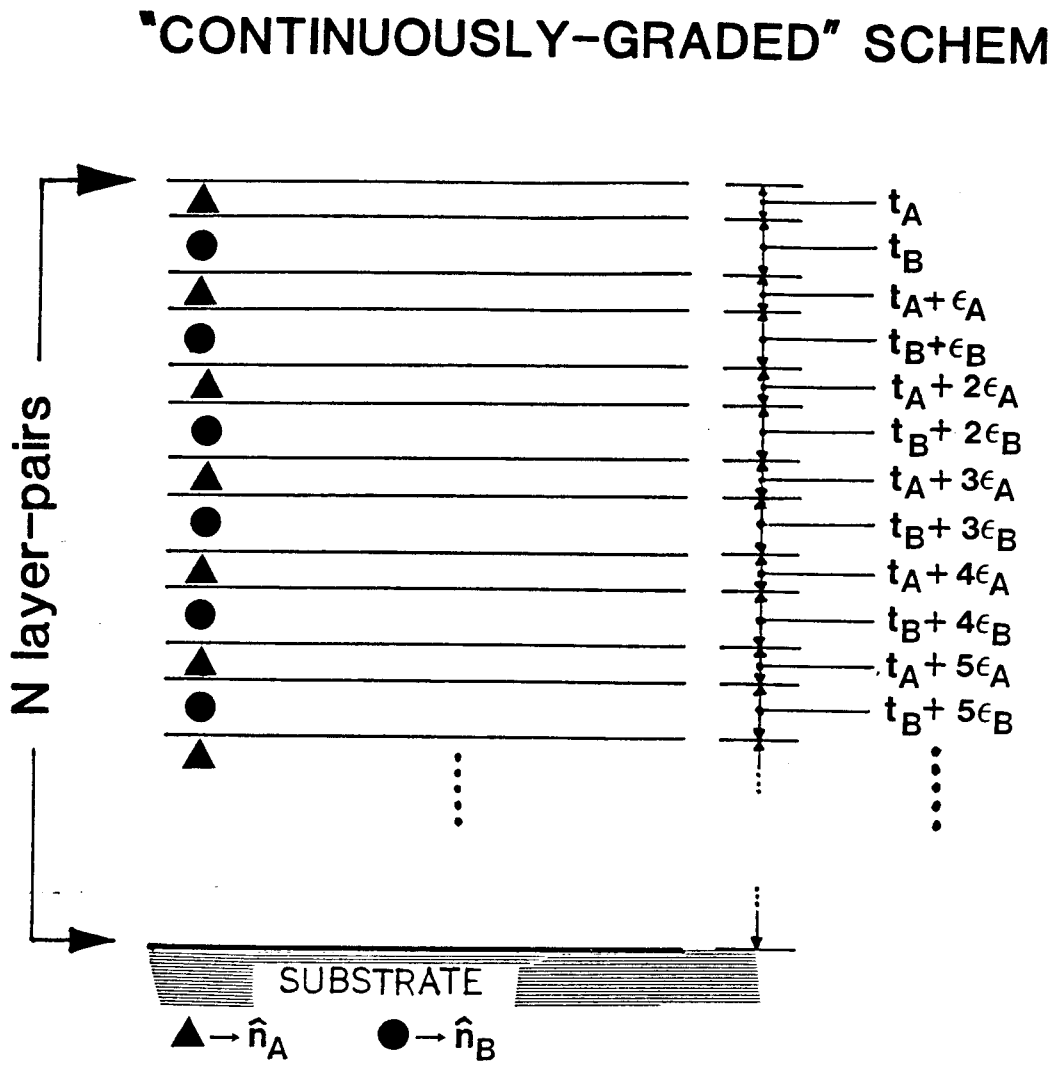
"CONTINUOUSLY-GRADED" SCHEME
N layer-pairs
t_A
t_B
$t_A+\epsilon_A$
$t_B+\epsilon_B$
$t_A+2\epsilon_A$
$t_B+2\epsilon_B$
$t_A+3\epsilon_A$
$t_B+3\epsilon_B$
$t_A+4\epsilon_A$
$t_B+4\epsilon_B$
$t_A+5\epsilon_A$
$t_B+5\epsilon_B$
SUBSTRATE
▲→ $\hat{n}_A$
●→ $\hat{n}_B$

Fig. 1

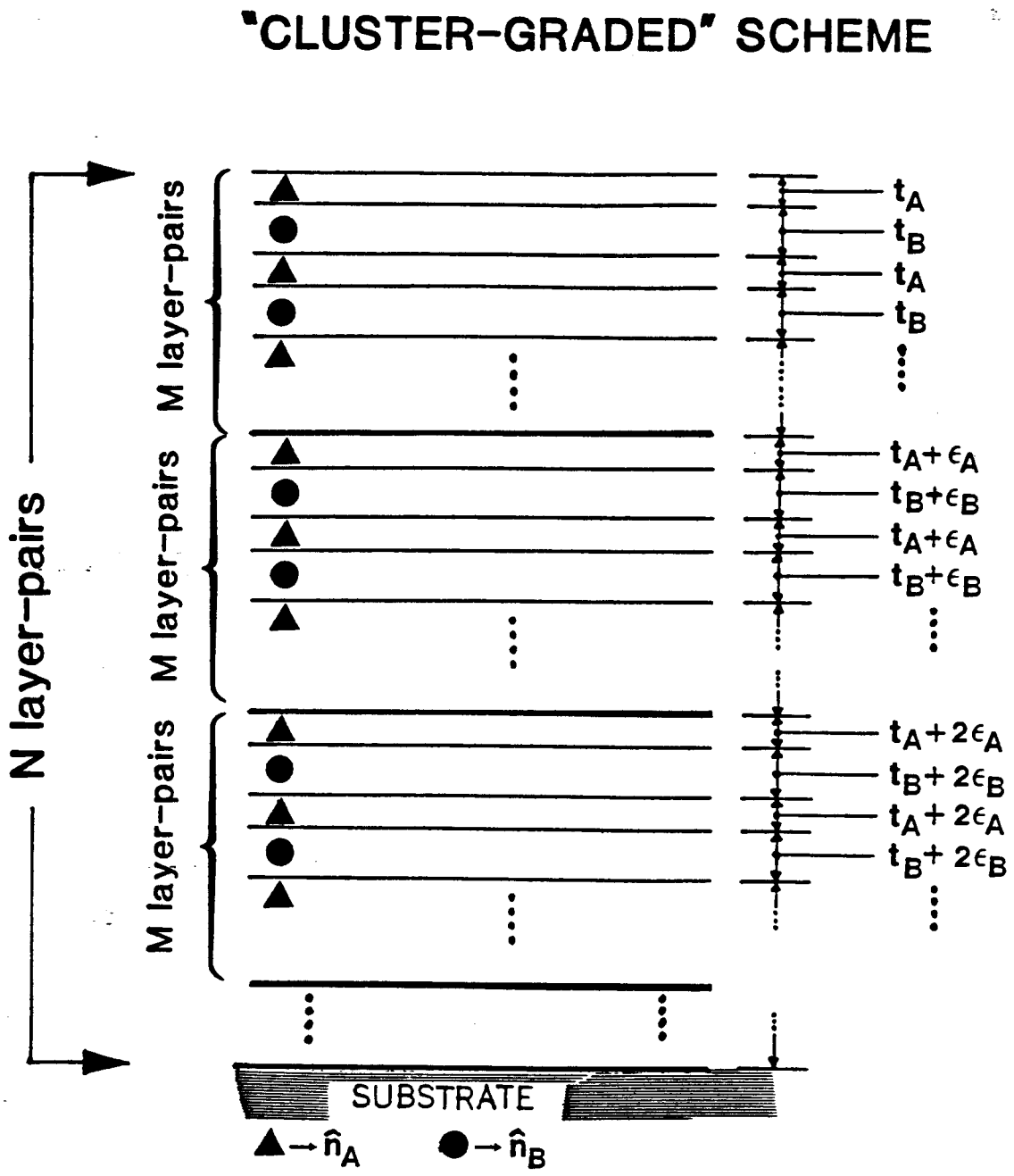
"CLUSTER-GRADED" SCHEME
N layer-pairs
M layer-pairs
M layer-pairs
M layer-pairs
t_A
t_B
t_A
t_B
$t_A+\epsilon_A$
$t_B+\epsilon_B$
$t_A+\epsilon_A$
$t_B+\epsilon_B$
$t_A+2\epsilon_A$
$t_B+2\epsilon_B$
$t_A+2\epsilon_A$
$t_B+2\epsilon_B$
SUBSTRATE
$\hat{n}_A$
$\hat{n}_B$

Fig. 2

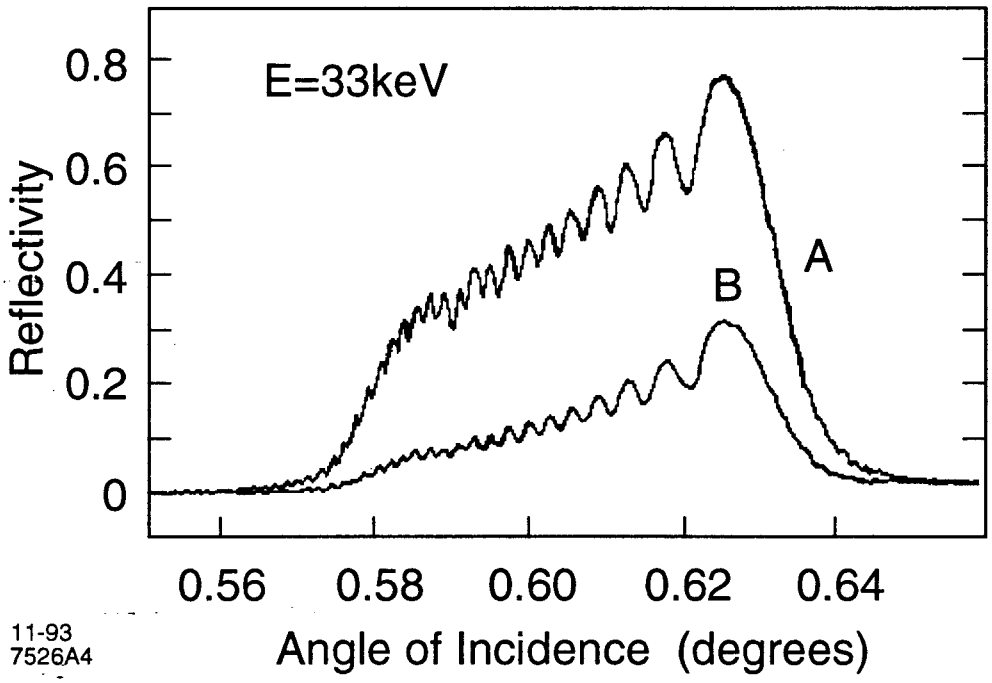
E=33keV
Reflectivity
0.8
0.6
0.4
0.2
0
A
B
0.56
0.58
0.60
0.62
0.64
Angle of Incidence (degrees)
11-93
7526A4

Fig. 3

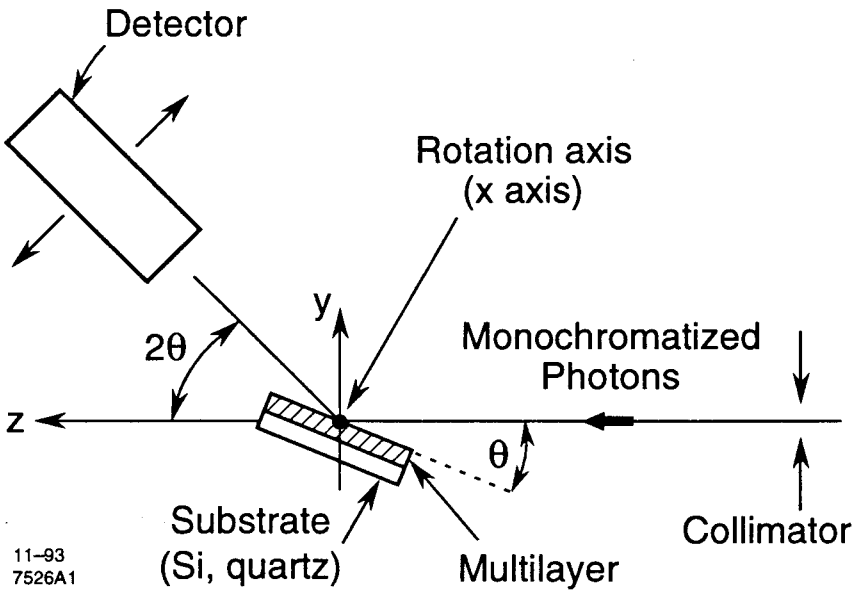
Detector
Rotation axis
(x axis)
y
2θ
Monochromatized
Photons
z
θ
Substrate
(Si, quartz)
Multilayer
Collimator
11–93
7526A1

Fig. 4

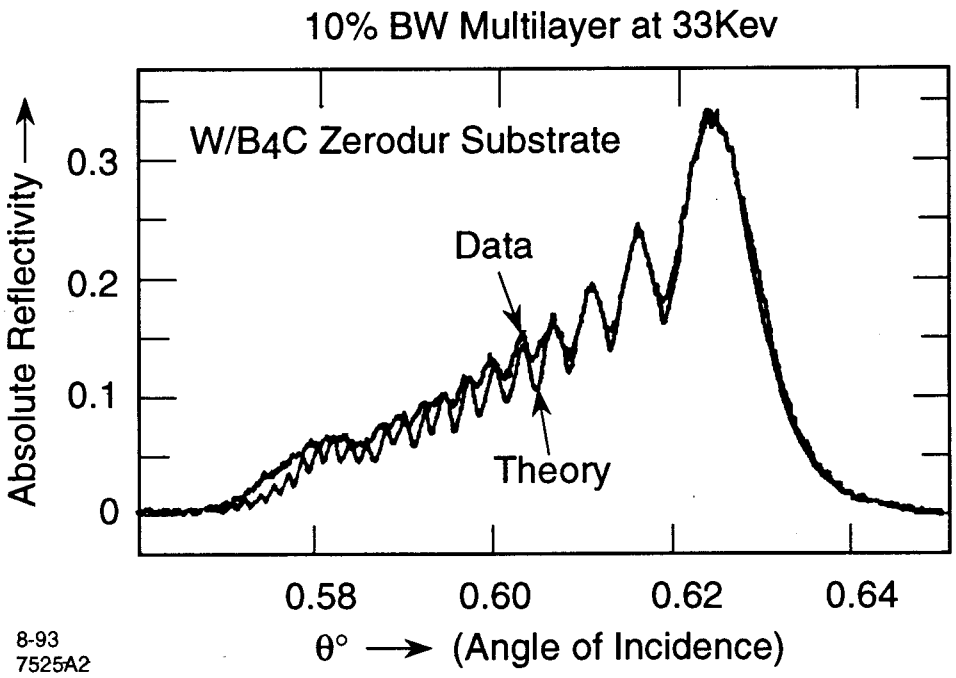
10% BW Multilayer at 33Kev
W/B4C Zerodur Substrate
Data
Theory
Absolute Reflectivity
0.3
0.2
0.1
0
0.58
0.60
0.62
0.64
θ° → (Angle of Incidence)
8-93
7525A2

Fig. 5

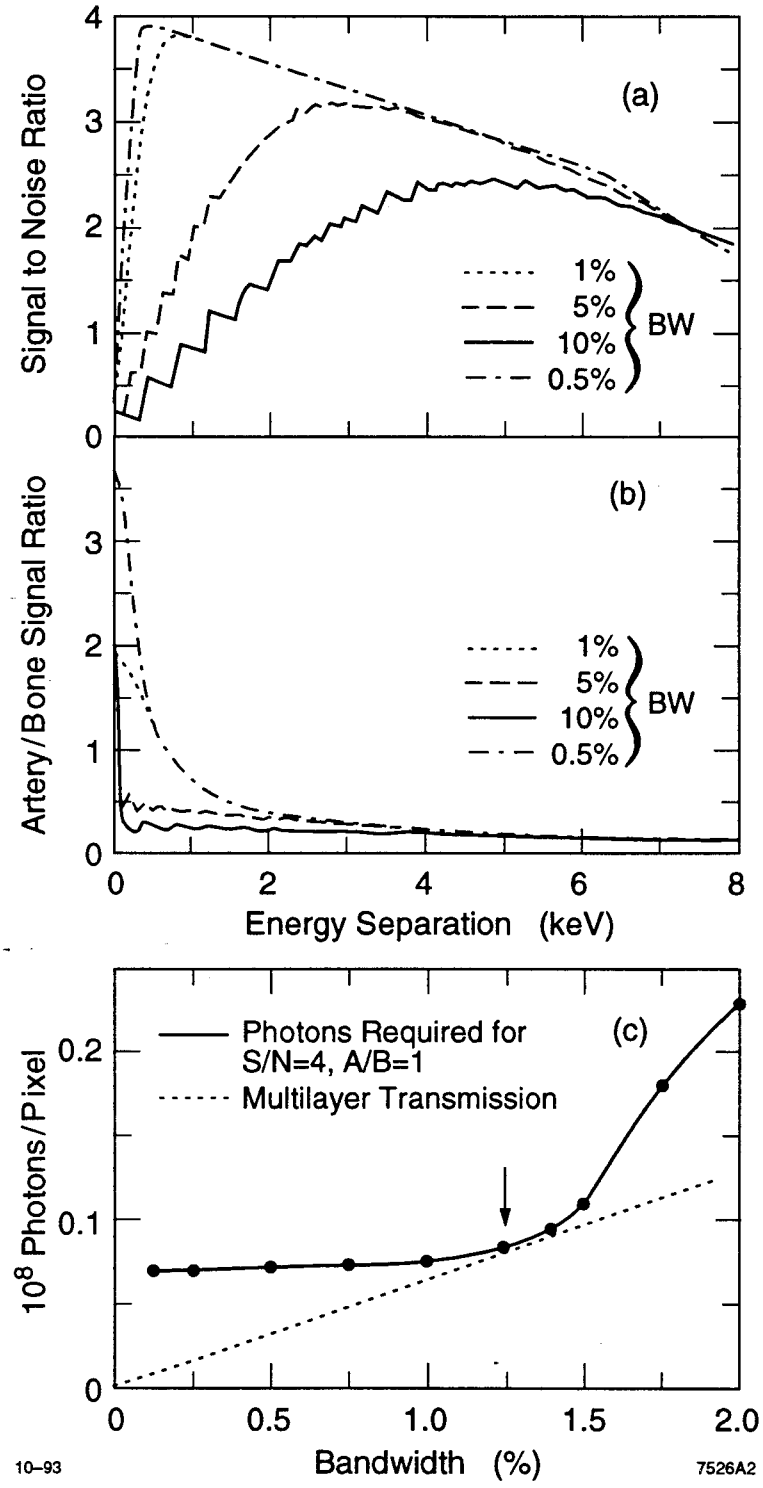
Signal to Noise Ratio
(a)
1%
5%
10%
0.5%
BW
Artery/Bone Signal Ratio
(b)
1%
5%
10%
0.5%
BW
Energy Separation (keV)
10^8 Photons/Pixel
Photons Required for S/N=4, A/B=1
Multilayer Transmission
(c)
Bandwidth (%)
10-93
7526A2

Fig. 6